

超声对不锈钢基体表面激光熔注 WC 增强颗粒分布的影响规律研究

姚喆赫^{1,2,3}, 王发博^{1,2,3}, 孙振强^{1,2,3}, 陈智君^{1,2,3}, Liu Rong⁴, 姚建华^{1,2,3*}

¹浙江工业大学激光先进制造研究院, 浙江 杭州 310023;

²浙江工业大学机械工程学院, 浙江 杭州 310023;

³高端激光制造装备省部共建协同创新中心, 浙江 杭州 310023;

⁴卡尔顿大学机械与航空航天工程系, 加拿大 渥太华 K1S 5B6

摘要 针对激光熔注 WC 涂层中增强颗粒聚集及熔注层开裂的问题, 将超声引入激光熔注过程, 在 316L 不锈钢基板上开展了不同送粉速率下的超声辅助激光熔注 WC 颗粒实验研究, 分别采用不同单元内 WC 颗粒的数密度与 Voronoi 单元面积的离散系数来评价 WC 颗粒的聚集位置与均布程度, 对比分析了超声对 WC 颗粒熔解程度、聚集位置、均布程度与熔注层裂纹的影响。结果表明: 无超声作用下且送粉速率较大时, WC 颗粒在熔注层两侧边缘聚集; 当送粉速率为 2~8 g/min 时, 超声作用下的 Voronoi 单元面积离散系数相比无超声作用时减小了 18.7%~43.5%。这表明超声可以显著改善 WC 颗粒的局部聚集现象, 提升 WC 颗粒的均布程度, 从而进一步抑制熔注层裂纹的萌生。

关键词 激光技术; 激光熔注; 超声; 颗粒分布; Voronoi 图; 裂纹

中图分类号 TG178 **文献标志码** A

DOI: 10.3788/CJL221114

1 引言

盾构机、石油钻机的高端装备的服役环境恶劣, 其刀盘、钻头核心部件易发生磨损、点蚀等表面损伤, 损伤件的报废换新造成了巨大的经济损失和资源浪费。面向核心部件的使役需求, 采用激光熔注技术^[1]将陶瓷颗粒增强体的高硬度、高强度、高熔点与金属基体的韧性相结合^[2], 制备表面性能优异的金属基颗粒增强型涂层^[3], 对于延长易损件的服役寿命、提高装备运行的可靠性以及促进我国高端装备制造业的发展具有重要意义。

激光熔注使用的增强颗粒与基体材料在密度、热膨胀系数等属性上差别较大^[4], 因此, 当涂层内的颗粒分布不均时, 将会在颗粒聚集处产生应力集中, 导致涂层易萌生裂纹^[5]。因而, 对熔注层增强颗粒分布进行有效调控成为当前的研究热点。Xu 等^[6]提出了一种摆动激光熔注方法, 该方法提高了铝合金激光熔注中 SiC 颗粒在熔注层中的分布均匀性; 实验结果显示, 在摆动激光熔注工艺下, 匙孔面积越大, SiC 颗粒的注入深度越大。Freiße 等^[7]研究了激光功率、扫描速度、送

粉速率对增强颗粒含量与分布的影响, 结果发现: 激光功率越小, 送粉速率越大, 熔注层颗粒的含量越高。基于此, Freiße 等提出了一种通过金相截面计算熔注层颗粒含量的方法。Wang 等^[8]研究了 WC 粒径对颗粒分布特征的影响, 结果发现: 当 WC 粒径为 2 μm 和 5 μm 时, 颗粒分布较为均匀; 随着 WC 粒径增加, 颗粒的体积分数与熔解程度相应增加。Volpp 等^[9]探究了三种不同颗粒在熔注层中的分布特征, 结果显示: 由于熔体的流动和浮力的影响, 颗粒在熔池中的分布状态主要取决于颗粒密度; TiB₂ 颗粒相较于 WC-Co、B₄C 两种颗粒的分布更加均匀。Hu 等^[10]将 Ta 作为 NiCuBSi+WC 复合颗粒的增强相在 5Cr5MoSiV1 钢表面制备耐磨涂层, 结果发现: Ta 的加入消耗了涂层中的部分球形 WC 颗粒, 合成了原位 TaC, 并生成了均匀分布在涂层中的长棒状 W₂C 颗粒。康瑞泉等^[11]将稀土元素添加到镍基涂层中, 结果发现 Y₂O₃ 的添加显著提高了复合碳化物的数量与均匀度。Wang 等^[12]采用电磁场辅助激光熔注对熔注层颗粒的分布进行调控, 结果显示: 当由电磁复合场引起的定向洛伦兹力与重力方向相同时, 大部分颗粒分布在熔注层上部; 当洛

收稿日期: 2022-09-28; 修回日期: 2022-08-08; 录用日期: 2022-10-17; 网络首发日期: 2022-11-04

基金项目: 国家自然科学基金(52175443, U1809220)、浙江省属高校基本科研业务费专项资金(RF-B2020002)、浙江省公益技术应用研究项目(LGJ20E050002)

通信作者: *laser@zjut.edu.cn

伦兹力与重力方向相反时,多数颗粒分布在熔注层底部。胡勇等^[13]在制备 WC/316L 复合涂层时采用稳态磁场来抑制熔池流动,降低了颗粒的运动能力,制备了颗粒集中分布在上表层的梯度涂层。

综上所述,当前研究中采用的颗粒分布调控方法主要有 4 种:1) 调控工艺;2) 优化材料;3) 添加增强相或稀土元素;4) 外加能场。其中,外加能场的调控方法在拓宽工艺窗口、提升熔注层性能方面有着显著优势。超声在熔池中产生的声空化^[14]和声流效应^[15]在组织调控^[16]、缺陷抑制^[17]、性能提升^[18]等方面具有显著作用,已被应用于激光熔覆^[19-20]与激光焊接^[21-22]等领域。Wang 等^[23]、Xu 等^[24]等研究了超声对激光熔注层相结构、组织形貌、晶粒尺寸等微观组织的影响;Biswas 等^[25]、Gao 等^[26]等研究了超声对激光熔注层显微硬度、表面粗糙度、摩擦磨损性能等的影响。然而,当前研究中涉及超声对激光熔注增强颗粒分布影响的报道较少,影响的内在机理尚不明晰,同时有关颗粒分布状态的表征与评价方法较为欠缺,仍需进一步深入研究。基于此,本课题组将超声作为外加能场耦合作用于激光熔注过程,用于实现增强颗粒的分布调控;同时,基于样方与 Voronoi 图的分割方法对 WC 颗粒的聚集位置与均布程度进行了评价,分析了超声对熔注层颗粒分布的影响规律,并进一步揭示了超声对熔注层裂纹的抑制机理。

2 实验材料与方法

2.1 实验设备

实验采用的超声辅助激光熔注实验系统如图 1 所示,主要包括光纤耦合半导体激光器(Laserline LDF400-2000)、冷却系统、运动控制系统(IRB2400/16 型六轴机器人)、送粉器与超声台等装置。激光器的最大输出功率为 2000 W,输出波长范围为 900~

1070 nm,焦距为 21 mm,焦距处的激光光斑是直径为 4 mm 的圆形光斑,光斑范围内的能量分布为平顶高斯分布;超声装置的输出功率在 50~5000 W 范围内可调,频率为 20 kHz;送粉气与保护气均为氩气。

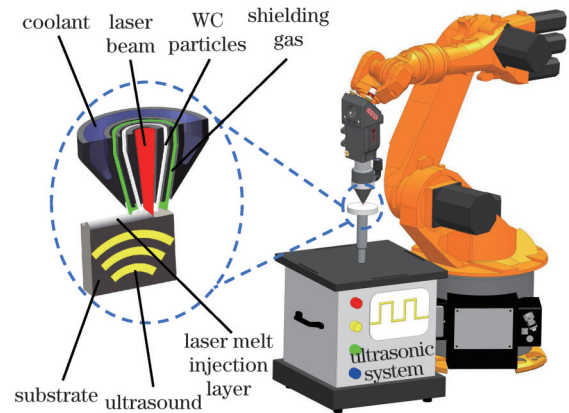


图 1 超声辅助激光熔注实验平台

Fig. 1 Experimental setup for ultrasonic-assisted laser melt injection

2.2 实验材料

实验所用基体是尺寸为 $\Phi 100 \text{ mm} \times 4.8 \text{ mm}$ 的 316L 不锈钢板。在开展激光熔注实验前,将基板打磨至平整光亮,并用乙醇对基板进行清洗,以去除其表面的污渍。熔注所用颗粒为球形 WC 颗粒,其显微形貌及粒径统计结果如图 2 所示。颗粒粒径整体呈正态分布,均值约为 $75 \mu\text{m}$ 。对熔注颗粒进行 X 射线衍射(XRD)测试(电压为 40 kV,电流为 40 mA,模式为 Continuous,步长为 0.02° , 2θ 角范围为 $20^\circ \sim 80^\circ$,扫描速率为 $5^\circ/\text{min}$)以确定其物相,测试结果如图 2 所示。图 2 显示实验所用颗粒由 WC、 W_2C 两种相组成。实验开始前,将熔注颗粒置于保温炉中进行干燥处理,保温温度为 120°C ,保温时间为 1 h。

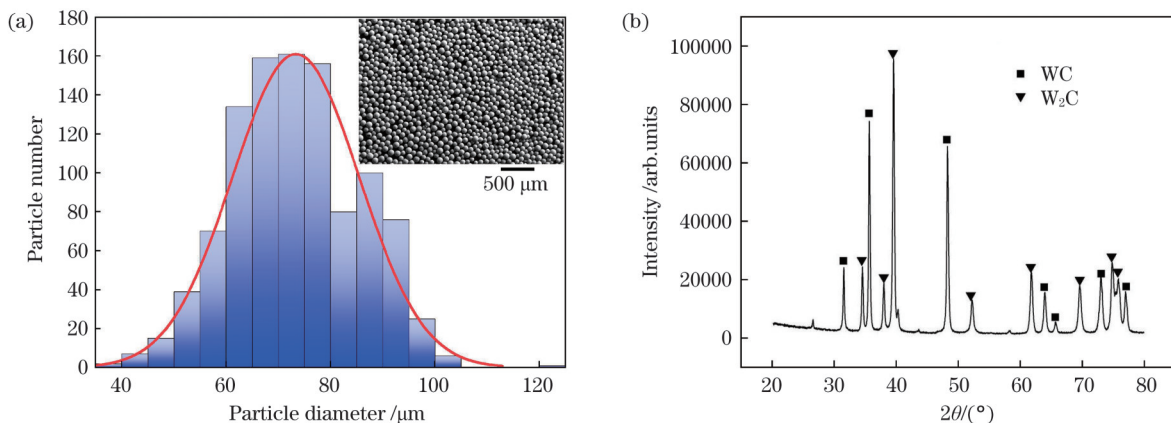


图 2 WC 颗粒的显微形貌、粒径统计及物相组成。(a) WC 颗粒的形貌与粒径分布;(b) WC 颗粒的 XRD 测试结果

Fig. 2 Morphology, particle size and phase composition of WC particles. (a) Morphology and size distribution of WC particles; (b) XRD test result of WC particles

2.3 实验方案

基于图 1 所示的实验平台开展有/无超声作用下

以及不同送粉速率下的激光熔注实验研究(超声频率为 20 kHz,超声功率为 3 kW),工艺参数如表 1 所示。

熔注实验结束后,采用 DPT-核着色渗透探伤喷剂进行探伤测试。探伤测试前先清洗熔注层表面,然后依次将渗透剂与显像剂喷涂在熔注层表面,对熔注层表面裂纹进行观察。探伤测试后,分别取熔注层的横截

面(垂直于激光扫描方向)试样与纵截面(平行于激光扫描方向)试样,试样经抛光、腐蚀后,采用蔡司 Axioscope 光学显微镜对熔注层中的 WC 颗粒分布进行观察与分析。

表 1 超声辅助激光熔注实验的工艺参数

Table 1 Process parameters of ultrasonic-assisted laser melt injection

Specimen No.	Laser power /W	Scanning speed / (mm·s ⁻¹)	Powder feeding rate / (g·min ⁻¹)	With or without ultrasound
a	1600	8	2	Without
b	1600	8	2	With
c	1600	8	4	Without
d	1600	8	4	With
e	1600	8	6	Without
f	1600	8	6	With
g	1600	8	8	Without
h	1600	8	8	With

3 结果与讨论

3.1 超声对 WC 颗粒熔解程度的影响

对送粉速率为 8 g/min 时有/无超声作用下的熔注层纵截面形貌及纵截面中的 WC 颗粒粒径进行统计分析,统计结果如图 3 所示。可见,熔注层中的 WC 颗粒

粒径整体呈正态分布,有/无超声作用下的粒径均值相近,均约为 45 μm(与熔注前的原始粒径相比降低了约 30 μm)。在前期研究^[27]中用热电偶测量了超声热效应导致的温升,结果显示,超声热效应导致的温升与熔池温度相比可以忽略。因此,有/无超声作用下熔注层中 WC 颗粒的直径无显著差别。

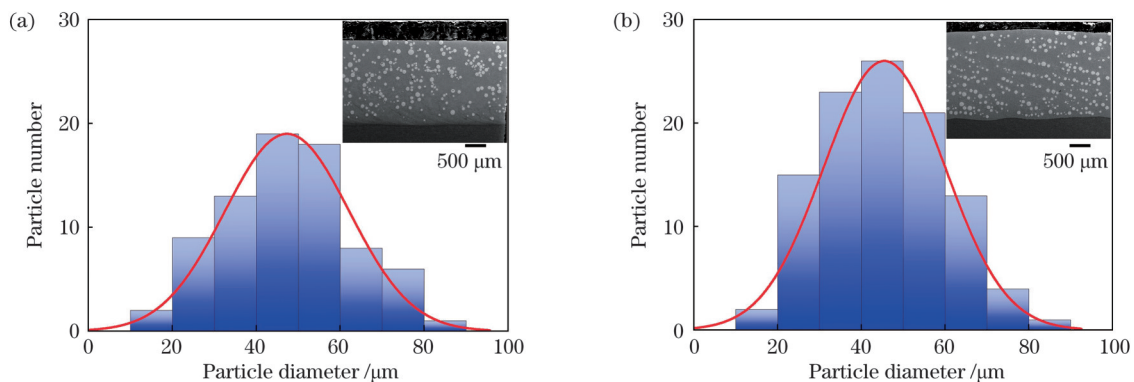


图 3 送粉速率为 8 g/min 时熔注层的纵截面形貌以及纵截面上的 WC 颗粒粒径分布。(a) 无超声作用;(b) 有超声作用

Fig. 3 Longitudinal section morphology and WC particle size distribution on longitudinal section of laser melt injection layer with a powder feeding rate of 8 g/min. (a) Without ultrasound; (b) with ultrasound

3.2 超声对 WC 颗粒聚集位置的影响

对比了送粉速率为 8 g/min 时有/无超声作用下的熔注层横截面形貌,结果发现无超声作用下的 WC 颗粒在熔注层横截面两侧边缘出现了明显的聚集现象,如图 4 所示。为进一步分析 WC 颗粒在熔注层横截面不同位置的聚集情况,提取了熔注层的横截面轮廓以及 WC 颗粒的中心点,以熔注层横截面底部最低点为原点,以水平向右为 x 轴正向,以竖直向上为 y 轴正向,以 300 μm 为步长绘制网格,将熔注层横截面划分成多个单元,如图 4 所示。定义单元内 WC 颗粒的数密度 C 为

$$C = n/\alpha, \quad (1)$$

式中: n 为单元内 WC 颗粒的数目; α 为单元面积与矩

形网格面积($9 \times 10^4 \mu\text{m}^2$)的比值。

不同单元中 WC 颗粒的数密度如图 5 所示。结合三维柱状图可以直观地发现:在无超声作用下,共划分了 47 个单元,其中分布在两侧 10 个单元中的 WC 颗粒的数密度 ≥ 10 ;在超声作用下,共划分了 50 个单元,其中仅 $(-6, 5)$ 单元中 WC 颗粒的数密度为 10,有 4 个单元中 WC 颗粒的数密度为 0,其余单元中 WC 颗粒的数密度在 2~9 之间。

基于样方^[28]方法对熔注层横截面进行分割,通过不同单元内颗粒的数密度对 WC 颗粒的聚集位置进行分析,分析结果显示:在无超声作用下,WC 颗粒聚集在熔注层横截面两侧边缘,熔注层横截面中部的 WC

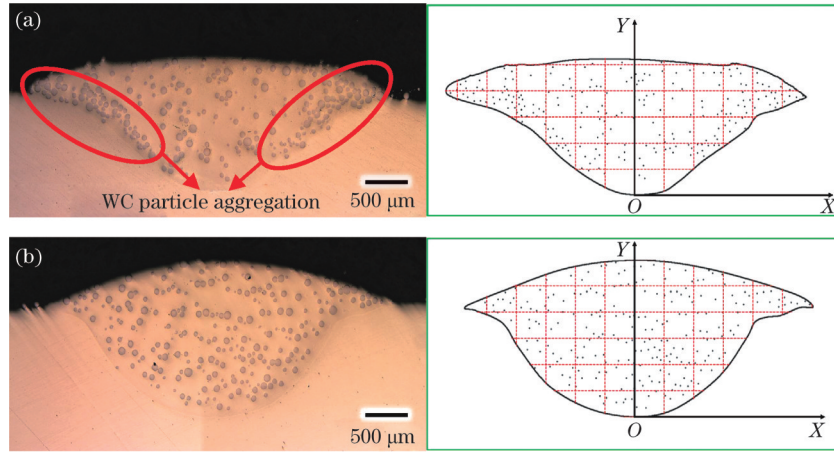


图 4 送粉速率为 8 g/min 时熔注层的纵横截面形貌以及单元划分。(a) 无超声作用; (b) 有超声作用

Fig. 4 Cross section morphology and cell division of laser melt injection layer with powder feeding rate of 8 g/min. (a) Without ultrasound; (b) with ultrasound

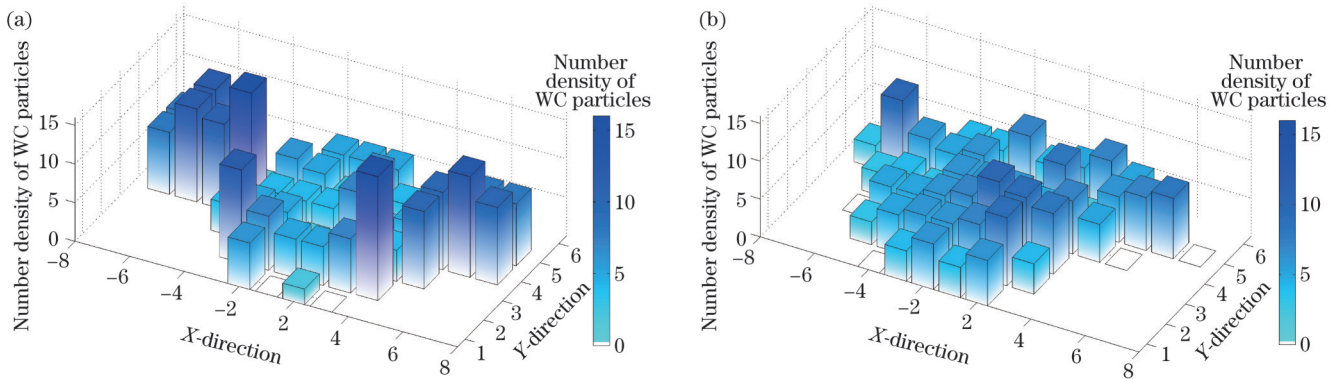


图 5 送粉速率为 8 g/min 时不同单元中 WC 颗粒的数密度。(a) 无超声作用; (b) 有超声作用

Fig. 5 Number density of WC particles in different cells with a powder feeding rate of 8 g/min. (a) Without ultrasound; (b) with ultrasound

颗粒数量明显少于两侧;在超声作用下,WC 颗粒在熔注层横截面不同位置处的数量相近,无明显的聚集现象。样方方法简便直观地呈现了 WC 颗粒在熔注层横截面上的聚集位置,说明单一激光熔注在送粉速率较大时存在 WC 颗粒易在熔注层两侧边缘聚集的现象。然而,此方法较为依赖网格度量与指标稳健性^[29],在不同的送粉速率下熔注层内部颗粒数量差异较大,难以选取统一的网格度量对不同送粉速率下的试样进行对比分析。

3.3 超声对 WC 颗粒均布程度的影响

为了对不同送粉速率下 WC 颗粒的分布进行量化分析,以 WC 颗粒的中心为基点,以熔注层横截面轮廓为边界,构建了熔注层 Voronoi 图。Voronoi 图是一种空间分割算法^[30],其数学定义为:对于给定平面上的有限数量点集 $x = \{x_1, x_2, \dots, x_n\}$, $d(x, x_i)$ 为点 x 与点 x_i 在给定平面上的欧氏距离, Ω_i^{Vor} 为基点 x_i 所对应的 Voronoi 单元,则 Ω_i^{Vor} 内任意一点 x 到该 Voronoi 单元基点的距离小于其到其他任意基点的距离^[31],即

$$\Omega_i^{Vor} = \{x | d(x, x_i) < d(x, x_j), j \neq i\}, \quad (2)$$

相应的点集 x 的 Voronoi 图为

$$\Omega_x^{Vor} = \{\Omega_1^{Vor}, \Omega_2^{Vor}, \dots, \Omega_n^{Vor}\}. \quad (3)$$

熔注层 Voronoi 图的构建流程如图 6 所示。对熔注层横截面的光镜图像进行二值化处理,然后提取熔注层横截面轮廓与 WC 颗粒轮廓并采用图像一阶矩计算 WC 颗粒的中心点,接着以 WC 颗粒的中心点为基点,以熔注层横截面轮廓为边界构建熔注层 Voronoi 图。统计图像中各 Voronoi 单元的面积。

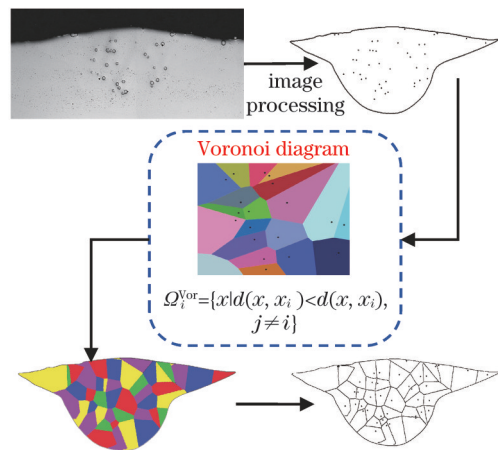


图 6 熔注层 Voronoi 图的构建流程

Fig. 6 Construction process for Voronoi diagram of laser melt injection layer

分别对有无超声下送粉速率分别为 2、4、6、8 g/min 的熔注层横截面构建 Voronoi 图并绘制对应的

Voronoi 单元面积分布图, 结果如图 7 和图 8 所示。分析后发现所有工艺参数下的 Voronoi 单元面积分布理

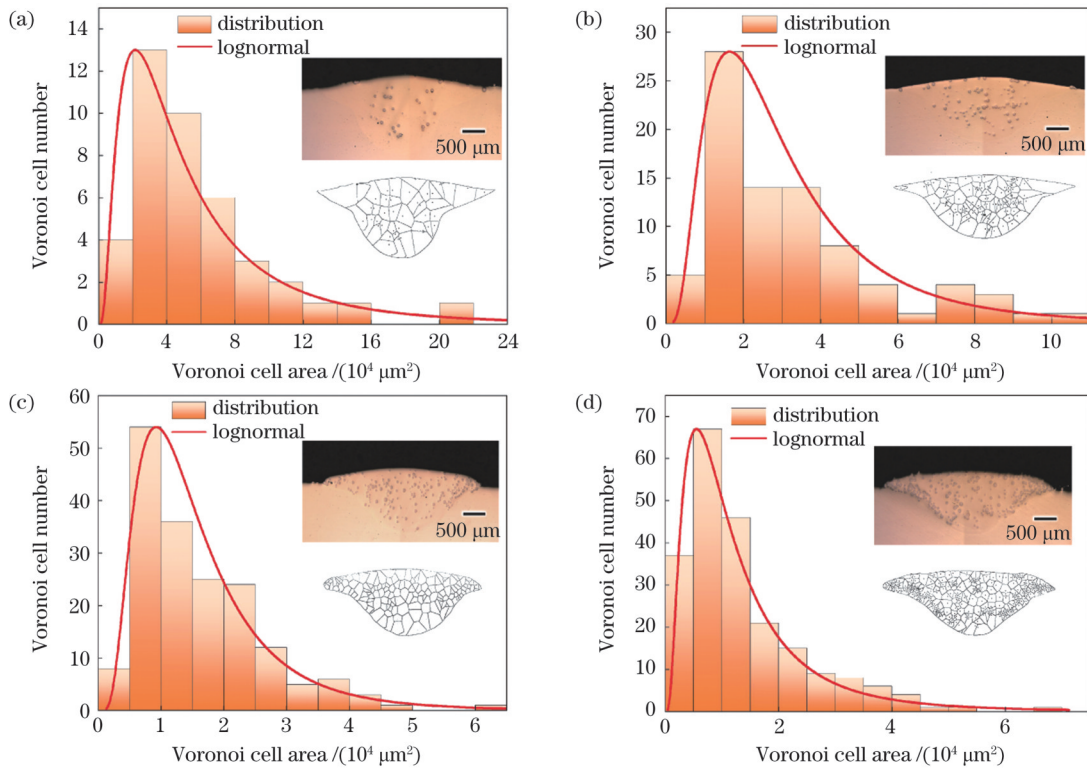


图 7 无超声作用下熔注层的 Voronoi 单元面积。(a) 送粉速率 2 g/min; (b) 送粉速率 4 g/min; (c) 送粉速率 6 g/min; (d) 送粉速率 8 g/min
 Fig. 7 Voronoi cell area of laser melt injection layer without ultrasound. (a) Powder feeding rate of 2 g/min; (b) powder feeding rate of 4 g/min; (c) powder feeding rate of 6 g/min; (d) powder feeding rate of 8 g/min

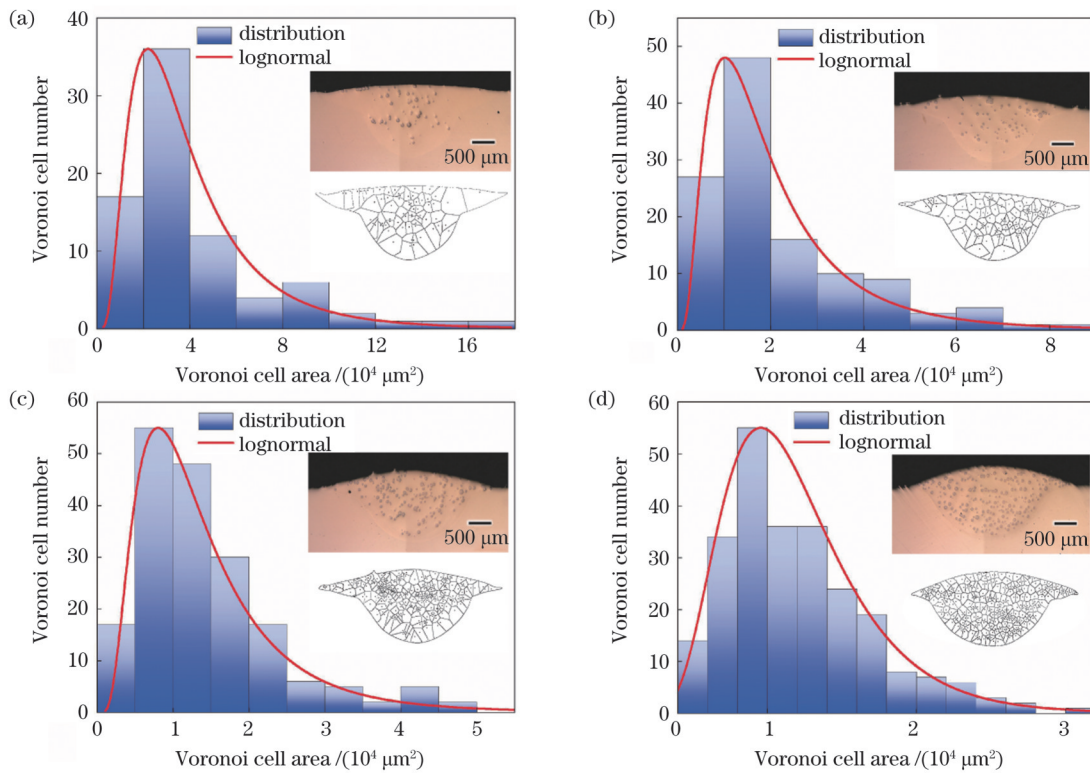


图 8 超声作用下熔注层 Voronoi 单元面积。(a) 送粉速率 2 g/min; (b) 送粉速率 4 g/min; (c) 送粉速率 6 g/min; (d) 送粉速率 8 g/min
 Fig. 8 Voronoi cell area of laser melt injection layer with ultrasound. (a) Powder feeding rate of 2 g/min; (b) powder feeding rate of 4 g/min; (c) powder feeding rate of 6 g/min; (d) powder feeding rate of 8 g/min

论上均符合对数正态分布^[32]。为了方便比较分析,提取拟合得到的对数正态分布曲线,并绘制在同一坐标系下,如图 9 所示。观察图 9 可以直观地发现在送粉速率增加与超声的共同作用下,拟合对数曲线逐渐由“平缓”变得“陡峭”,Voronoi 单元面积分布区间由 $0 \sim 10^5 \mu\text{m}^2$ 显著减小至 $0 \sim 10^4 \mu\text{m}^2$ 。

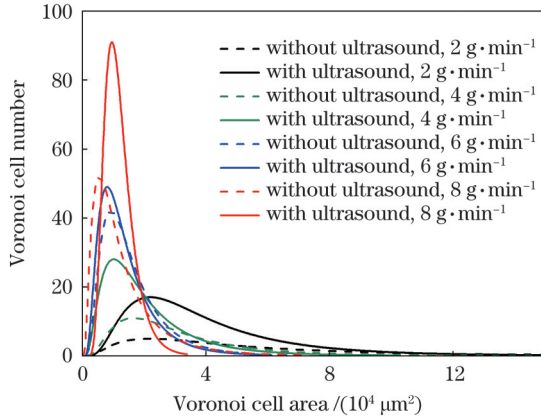


图 9 Voronoi 单元面积的对数正态分布拟合曲线
Fig. 9 Fitting lognormal curve of Voronoi cell area

以 Voronoi 单元面积为度量^[33],以 Voronoi 单元面积的离散系数 c_v 来评价熔注层中 WC 颗粒的均布程度 (c_v 越小,表示 WC 颗粒的分布越均匀)。离散系数 c_v 的计算公式为

$$c_v = \sigma_x / \bar{x}, \quad (4)$$

式中: σ_x 为 Voronoi 单元面积标准差; \bar{x} 为 Voronoi 单元面积均值。对有/无超声时不同送粉速率下的试样分别截取 3 个横截面进行分析,计算 Voronoi 单元面积的离散系数 c_v ,计算结果如图 10 所示。由图 10 可以发现:无论有/无超声作用,送粉速率的增加均会使 Voronoi 单元面积的离散系数 c_v 减小。但正如前文所述,无超声作用时,送粉速率的增加会导致 WC 颗粒在熔注层两侧边缘聚集,而超声则显著改变了这一现象,使得离散系数 c_v 进一步减小,WC 颗粒的均布程度提升;而且随着送粉速率增加,超声的效果不断增强,送

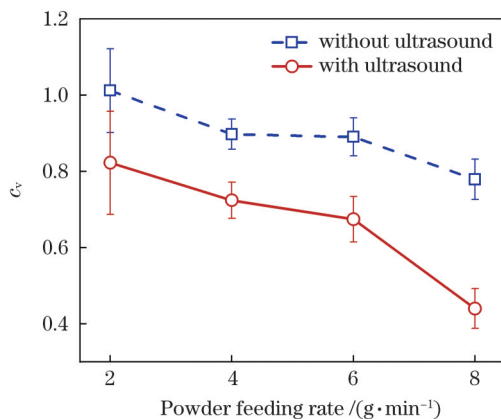


图 10 熔注层 Voronoi 单元面积的离散系数

Fig. 10 Coefficient of variability of Voronoi cell area of laser melt injection layer

粉速率为 2、4、6、8 g/min 时的离散系数 c_v 相比无超声作用时分别减小了 18.7%、19.3%、24.3%、43.5%。

基于上述分析可知,当送粉速率较小时,熔注层内部的 WC 颗粒较少,空间利用率不足,WC 颗粒集中在截面中部,导致以边角处 WC 颗粒为基点的 Voronoi 单元面积过大。以无超声时送粉速率为 2 g/min 的试样为例,其最大 Voronoi 单元面积为 $2.4 \times 10^5 \mu\text{m}^2$,而多数 Voronoi 单元面积集中在 $4 \times 10^4 \sim 8 \times 10^4 \mu\text{m}^2$ 之间。送粉速率的增加导致熔注层中 WC 颗粒增加,熔池的空间利用率提升,大幅减少了面积过大的 Voronoi 单元,从而提升了熔注层内 WC 颗粒的均布程度。超声提升颗粒均布程度的机制在于:1) 超声提升了熔注层内部颗粒的数量,减少了面积过大的 Voronoi 单元;2) 超声显著改善了熔注层两侧边缘 WC 颗粒的聚集,减少了面积过小的 Voronoi 单元。当送粉速率为 2、4 g/min 时,颗粒均布程度主要受第一种机制的影响;当送粉速率为 6、8 g/min 时,颗粒均布程度受两种机制的共同影响。

在激光熔注过程中,熔池内 WC 颗粒的运动过程决定着其在熔注层中的最终分布状态。颗粒运动过程主要受浮力、重力、拖曳力三者的共同影响。其中,熔池中的流体对 WC 颗粒的拖曳力 F_d ^[34] 可以表示为

$$F_d = \frac{1}{6\tau_p} \pi d_p^3 \rho_p (u_f - u_p), \quad (5)$$

式中: τ_p 为颗粒弛豫时间; d_p 为颗粒直径; ρ_p 为基板材料熔体的密度; u_f 为熔池中流体的流速; u_p 为颗粒的流速。激光熔注过程中,在温度梯度与表面张力差异的共同作用下,熔池内部会呈现出对称分布的自外向内流动的双涡流结构^[35]。WC 颗粒的密度 (16500 kg/m^3) 与 316L 不锈钢的密度 (6881 kg/m^3) 相差较大,因此,当送粉速率较大时,熔池内部大量的 WC 颗粒会抑制熔池的流动,使熔池的流速 u_f 减小,WC 颗粒所受拖曳力 F_d 减小,导致 WC 颗粒在重力的主导下运动至熔池两侧固/液界面并被捕获;随着凝固的进行,大量 WC 颗粒聚集在熔注层两侧边缘。超声产生的声空化与声流效应可以显著促进熔池流动,增大熔池的环流速度,WC 颗粒在较大拖曳力的作用下随着环流从熔池两侧向熔池中心运动,从而改善了 WC 颗粒的聚集,提升了 WC 颗粒的均布程度。

3.4 超声对熔注层裂纹分布的影响

制备的激光熔注 WC 增强涂层内部含有大量的高脆性 WC 颗粒以及由 WC 颗粒熔解产生的 C、W 元素结合而成的高脆性组织,导致熔注层易萌生裂纹,严重影响了成形件的性能。为此,本课题组开展了熔注层探伤测试,分析了超声对熔注层裂纹的影响规律。探伤结果如图 11 所示。可以发现:送粉速率 (2、4 g/min) 较小时,有/无超声作用下的熔注层中均无裂纹产生;当送粉速率达到 6 g/min 时,无超声作用下的熔注层开始出现宏观裂纹;在超声作用下,熔注层在送粉速率

达到 8 g/min 时才开始出现宏观裂纹, 并且裂纹数目较少。

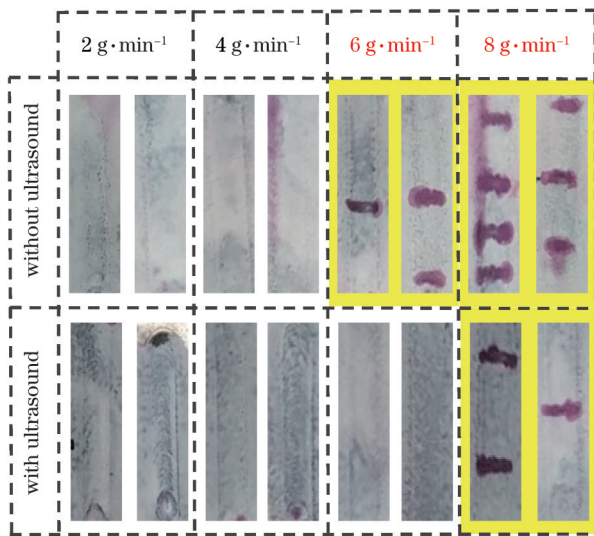


图 11 有无超声作用下的熔注层探伤图

Fig. 11 Flaw detection of laser melt injection layer with and without ultrasound

有/无超声辅助及不同送粉速率下熔注层中裂纹的分布及形貌如图 12 所示。本研究选取的基体材料(316L 不锈钢)具有较好的韧性, 因此, 当无超声作用且送粉速率为 6、8 g/min 时, 以及有超声作用且送粉速率为 8 g/min 时, 产生的宏观裂纹均贯穿了整个熔覆层并止于熔合线附近。图 12(b) 为无超声作用且送粉速率为 6 g/min 时熔注层横截面的裂纹萌生与扩展

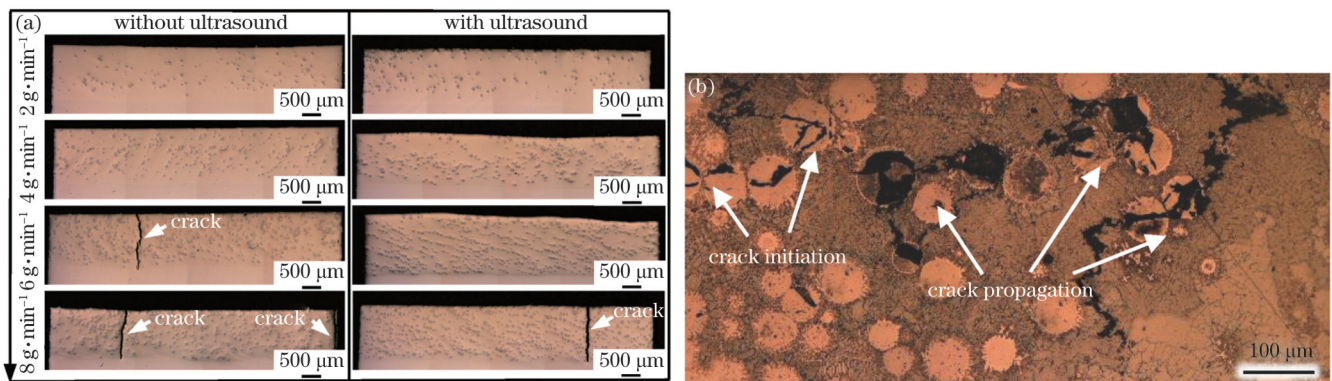


图 12 熔注层中裂纹的分布及形貌。(a)纵截面;(b)横截面

Fig. 12 Distribution and morphology of crack in laser melt injection layer. (a) Longitudinal section; (b) cross section

4 结 论

采用超声辅助激光熔注在 316L 不锈钢表面制备了 WC 颗粒强化层, 并对熔注层内 WC 颗粒的熔解程度、聚集位置、均布程度以及熔注层裂纹进行了分析。结果表明: 当送粉速率为 8 g/min 时, 无超声作用下 WC 颗粒在熔注层两侧边缘存在着显著的聚集现象, 熔注层存在较多宏观裂纹; 超声改善了 WC 颗粒的局部聚集现象, 提升了 WC 颗粒的均布程度; 当送粉速率

情况, 可以发现: 随着 WC 颗粒的聚集, 裂纹最初萌生在 WC 颗粒内部^[5], 随后裂纹沿着由 WC 颗粒溶解生成的大量高脆性组织扩展, 最终形成宏观裂纹。

激光熔注增强涂层中的应力集中是裂纹产生的主要原因之一, 增强颗粒与基体材料热膨胀系数等物性参数的不同^[36-37]、增强颗粒聚集与分布不均^[38]等都会导致应力集中。研究表明: 颗粒聚集可以缩短颗粒之间的平均距离, 增加应力集中程度^[39]; 颗粒聚集也可以诱导微结构应力的形成^[40]; WC 颗粒的局部聚集将产生位错塞积群, 从而导致应力集中^[41]。在无超声作用下, 当送粉速率为 6 g/min 或 8 g/min 时, 随着熔注层中 WC 颗粒不断增多, WC 颗粒逐渐聚集在熔注层的两侧, 造成应力集中; 当应力以及 WC 颗粒与基体之间的热膨胀失配系数大于 WC 的屈服强度时, 裂纹就会在 WC 颗粒内部萌生^[42-43]并沿着高脆性组织不断扩展^[40]。在超声作用下, 送粉速率为 6 g/min 的熔注层中无明显裂纹产生。结合上述分析可知这是因为超声产生的声流效应与声空化效应促进了 WC 颗粒的均匀分布, 避免了 WC 颗粒局部聚集导致的颗粒平均距离过小、微结构应力与位错塞积, 从而避免了应力集中, 抑制了裂纹的产生。但当送粉速率增加到 8 g/min 时, 即便是超声作用下熔注层中 WC 颗粒的分布较为均匀, 仍出现了裂纹。分析认为这是由于 WC 颗粒大量增加后, 熔池中熔解的 C、W 元素增多, 最终熔池凝固时产生了大量的高脆性组织, 导致熔注层的脆性急剧增加, 从而导致裂纹产生。

为 2~8 g/min 时, 超声作用下的 Voronoi 单元面积的离散系数相比无超声作用时减小了 18.7%~43.5%, 超声作用下 WC 颗粒均布程度的提升抑制了熔注层裂纹的萌生, 使得超声作用下的熔注层裂纹数量显著减少。

参 考 文 献

- [1] Ayers J D. Wear behavior of carbide-injected titanium and aluminum alloys[J]. *Wear*, 1984, 97(3): 249-266.
- [2] Verezub O, Kálazi Z, Buza G, et al. *In-situ* synthesis of a carbide

- reinforced steel matrix surface nanocomposite by laser melt injection technology and subsequent heat treatment[J]. *Surface and Coatings Technology*, 2009, 203(20/21): 3049-3057.
- [3] Li L Q, Liu D J, Chen Y B, et al. Electron microscopy study of reaction layers between single-crystal WC particle and Ti-6Al-4V after laser melt injection[J]. *Acta Materialia*, 2009, 57(12): 3606-3614.
- [4] Farahmand P, Liu S, Zhang Z, et al. Laser cladding assisted by induction heating of Ni-WC composite enhanced by nano-WC and La_2O_3 [J]. *Ceramics International*, 2014, 40(10): 15421-15438.
- [5] Wang J D, Li L Q, Tao W. Crack initiation and propagation behavior of WC particles reinforced Fe-based metal matrix composite produced by laser melting deposition[J]. *Optics & Laser Technology*, 2016, 82: 170-182.
- [6] Xu B A, Jiang P, Wang Y L, et al. Multi-physics simulation of wobbling laser melting injection of aluminum alloy with SiC particles: SiC particles gradient distribution in fusion zone[J]. *International Journal of Heat and Mass Transfer*, 2022, 182: 121960.
- [7] Freiße H, Bohlen A, Seefeld T. Determination of the particle content in laser melt injected tracks[J]. *Journal of Materials Processing Technology*, 2019, 267: 177-185.
- [8] Wang Y Y, Gong Y F, Sun T F, et al. Effect of powder size and volume fraction of WC on the microstructure of laser cladding WC-NiCrBSi composite coatings[C]//2nd International Conference on Frontiers of Manufacturing and Design Science, December 11-13, 2011, Taichung, China. Switzerland: ICFMD, 2011: 105-109.
- [9] Volpp J, Dietz T, Vollertsen F. Particle property impact on its distribution during laser deep alloying processes[J]. *Physics Procedia*, 2014, 56: 1094-1101.
- [10] Hu D W, Liu Y, Chen H, et al. Microstructure and properties of Ta-reinforced NiCuBSi + WC composite coating deposited on 5Cr5MoSiV1 steel substrate by laser cladding[J]. *Optics & Laser Technology*, 2021, 142: 107210.
- [11] 康瑞泉, 刘文今, 马明星, 等. 稀土氧化物对激光熔覆制备颗粒增强镍基涂层中颗粒分布的影响[J]. *应用激光*, 2009, 29(5): 374-378.
- Kang R Q, Liu W J, Ma M X, et al. The effect of rare earth oxides on particle distribution in laser cladding particles reinforced Ni-base composite coatings[J]. *Applied Laser*, 2009, 29(5): 374-378.
- [12] Wang L, Yao J H, Hu Y, et al. Influence of electric-magnetic compound field on the WC particles distribution in laser melt injection[J]. *Surface and Coatings Technology*, 2017, 315: 32-43.
- [13] 胡勇, 王梁, 娄复兴, 等. 稳态磁场对激光熔注球形 WC 颗粒分布的影响机理研究[J]. *机械工程学报*, 2021, 57(1): 240-248.
- Hu Y, Wang L, Lou F X, et al. Mechanism study of steady magnetic field effect on spherical WC particle distribution during laser melt injection[J]. *Journal of Mechanical Engineering*, 2021, 57(1): 240-248.
- [14] Ida M, Naoe T, Futakawa M. Direct observation and theoretical study of cavitation bubbles in liquid mercury[J]. *Physical Review E*, 2007, 75(4): 046304.
- [15] Madelin G, Grucker D, Franconi J M, et al. Magnetic resonance imaging of acoustic streaming: absorption coefficient and acoustic field shape estimation[J]. *Ultrasonics*, 2006, 44(3): 272-278.
- [16] Zhang Y, Guo Y Q, Chen Y, et al. Microstructure and mechanical properties of Al-12Si alloys fabricated by ultrasonic-assisted laser metal deposition[J]. *Materials*, 2019, 13(1): 126.
- [17] Li M Y, Zhang Q, Han B, et al. Microstructure and property of Ni/WC/ La_2O_3 coatings by ultrasonic vibration-assisted laser cladding treatment[J]. *Optics and Lasers in Engineering*, 2020, 125: 105848.
- [18] Zhang D Z, Li Y Z, Wang H, et al. Ultrasonic vibration-assisted laser directed energy deposition *in situ* synthesis of NiTi alloys: effects on microstructure and mechanical properties[J]. *Journal of Manufacturing Processes*, 2020, 60: 328-339.
- [19] Gorunov A I, Nyukhlaev O A, Gilmutdinov A K. Investigation of microstructure and properties of low-carbon steel during ultrasonic-assisted laser welding and cladding[J]. *The International Journal of Advanced Manufacturing Technology*, 2018, 99(9): 2467-2479.
- [20] Ning F D, Hu Y B, Cong W L. Microstructure and mechanical property of TiB reinforced Ti matrix composites fabricated by ultrasonic vibration-assisted laser engineered net shaping[J]. *Rapid Prototyping Journal*, 2019, 25(3): 581-591.
- [21] Kolubaev A V, Sizova O V, Fortuna S V, et al. Weld structure of low-carbon structural steel formed by ultrasonic-assisted laser welding[J]. *Journal of Constructional Steel Research*, 2020, 172: 106190.
- [22] Tarasov S Y, Vorontsov A V, Fortuna S V, et al. Ultrasonic-assisted laser welding on AISI 321 stainless steel[J]. *Welding in the World*, 2019, 63(3): 875-886.
- [23] Wang X H, Liu S S, Zhao G L, et al. *In-situ* formation ceramic particles reinforced Fe-based composite coatings produced by ultrasonic assisted laser melting deposition processing[J]. *Optics & Laser Technology*, 2021, 136: 106746.
- [24] Xu W W, Bai X, Sun Z G, et al. Correlation between laser-ultrasound and microstructural properties of laser melting deposited Ti6Al4V/B₄C composites[J]. *Metals*, 2021, 11(12): 1951.
- [25] Biswas S, Alavi S H, Harimkar S P. Effect of laser remelting and simultaneous application of ultrasonic vibrations during laser melting on the microstructural and tribological properties of laser clad Al-SiC composites[J]. *Journal of Composites Science*, 2017, 1(2): 13.
- [26] Gao C, Wang Z, Xiao Z, et al. Selective laser melting of TiN nanoparticle-reinforced AlSi10Mg composite: microstructural, interfacial, and mechanical properties[J]. *Journal of Materials Processing Technology*, 2020, 281: 116618.
- [27] 卢习江. 超声辅助激光再制造 IN939 高温合金组织调控及性能研究[D]. 杭州: 浙江工业大学, 2020.
- Lu X J. Microstructure regulation and performance studies on ultrasonic assisted laser remanufacturing of IN939 superalloy[D]. Hangzhou: Zhejiang University of Technology, 2020.
- [28] Huang X H, Zhou Q, Zeng L, et al. Monitoring spatial uniformity of particle distributions in manufacturing processes using the K function[J]. *IEEE Transactions on Automation Science and Engineering*, 2017, 14(2): 1031-1041.
- [29] Kam K M, Zeng L, Zhou Q, et al. On assessing spatial uniformity of particle distributions in quality control of manufacturing processes [J]. *Journal of Manufacturing Systems*, 2013, 32(1): 154-166.
- [30] Brostow W, Dussault J P, Fox B L. Construction of Voronoi polyhedra[J]. *Journal of Computational Physics*, 1978, 29(1): 81-92.
- [31] Okabe A, Suzuki A. Locational optimization problems solved through Voronoi diagrams[J]. *European Journal of Operational Research*, 1997, 98(3): 445-456.
- [32] Peng Y H, Wang X G, Du Y, et al. Using Voronoi tessellation and Delaunay triangulation to evaluate spatial uniformity of particle distribution[J]. *Applied Mechanics and Materials*, 2014, 614: 413-416.
- [33] Zhu L B, Xiang X C, Du Y, et al. Uniformity assessment of TRISO fuel particle distribution in spherical HTGR fuel element using Voronoi tessellation and Delaunay triangulation[J]. *Science and Technology of Nuclear Installations*, 2018, 2018: 7274261.
- [34] 胡晓冬, 朱秀晖, 胡勇, 等. 稳态磁场对激光熔注尖角 WC 涂层颗粒分布及显微组织的影响[J]. *表面技术*, 2019, 48(2): 54-61.
- Hu X D, Zhu X H, Hu Y, et al. Effect of steady magnetic field on distribution and microstructure of sharp WC particle by laser melt injection[J]. *Surface Technology*, 2019, 48(2): 54-61.
- [35] 符永宏, 黄婷, 叶云霞, 等. 熔质流动特性对毛化凸点成形的影响[J]. *中国激光*, 2019, 46(7): 0702005.
- Fu Y H, Huang T, Ye Y X, et al. Influence of melt flow characteristics on textured bump forming[J]. *Chinese Journal of Lasers*, 2019, 46(7): 0702005.
- [36] Lee C M, Park H, Yoo J, et al. Residual stress and crack

- initiation in laser clad composite layer with Co-based alloy and WC + NiCr[J]. *Applied Surface Science*, 2015, 345: 286-294.
- [37] Zhou S F, Dai X Q, Zheng H Z. Microstructure and wear resistance of Fe-based WC coating by multi-track overlapping laser induction hybrid rapid cladding[J]. *Optics & Laser Technology*, 2012, 44(1): 190-197.
- [38] Aldas K, Mat M D. Experimental and theoretical analysis of particle distribution in particulate metal matrix composites[J]. *Journal of Materials Processing Technology*, 2005, 160(3): 289-295.
- [39] Zhou S F, Zeng X Y, Hu Q W, et al. Analysis of crack behavior for Ni-based WC composite coatings by laser cladding and crack-free realization[J]. *Applied Surface Science*, 2008, 255(5): 1646-1653.
- [40] Sun C J, Saffari P, Sadeghipour K, et al. Effects of particle arrangement on stress concentrations in composites[J]. *Materials Science and Engineering: A*, 2005, 405(1/2): 287-295.
- [41] Chen W T, Dickey E C. Indentation-induced deformation mechanisms in laser-processed directionally solidified WC-W₂C eutectoids[J]. *Journal of Materials Science*, 2017, 52(10): 5511-5519.
- [42] Liu D J, Chen Y B, Li L Q, et al. *In situ* investigation of fracture behavior in monocrystalline WC_p-reinforced Ti-6Al-4V metal matrix composites produced by laser melt injection[J]. *Scripta Materialia*, 2008, 59(1): 91-94.
- [43] Ignat S, Sallamand P, Nichici A, et al. MoSi₂ laser cladding: elaboration, characterisation and addition of non-stabilized ZrO₂ powder particles[J]. *Intermetallics*, 2003, 11(9): 931-938.

Effects of Ultrasound on Distribution of Laser Melt Injected WC Reinforced Particles on Stainless Steel Substrate Surface

Yao Zhehe^{1,2,3}, Wang Fabo^{1,2,3}, Sun Zhenqiang^{1,2,3}, Chen Zhijun^{1,2,3}, Liu Rong⁴, Yao Jianhua^{1,2,3*}

¹*Institute of Laser Advanced Manufacturing, Zhejiang University of Technology, Hangzhou 310023, Zhejiang, China;*

²*College of Mechanical Engineering, Zhejiang University of Technology, Hangzhou 310023, Zhejiang, China;*

³*Collaborative Innovation Center of High-End Laser Manufacturing Equipment (National "2011 Plan"), Hangzhou 310023, Zhejiang, China;*

⁴*Department of Mechanical and Aerospace Engineering, Carleton University, Ottawa K1S 5B6, Canada*

Abstract

Objective Core components of high-end equipment are prone to surface damage owing to harsh service environments. Reinforced coatings with great surface properties are able to be prepared via laser melt injection to prolong service life of core components. However, particles can easily locally aggregate during the process of laser melt injection, resulting in stress concentration and crack initiation in the coating layer. Presently, the approaches to control particle distribution mainly include process optimization, material optimization, adding reinforcement or rare earth elements, and applying external energy field. Because the acoustic cavitation and acoustic flow produced by the ultrasonic energy field in the molten pool have significant effects on microstructure regulation, defect suppression, and performance improvement, ultrasonic vibration has been applied to the fields of laser cladding and laser welding. Meanwhile, several studies on the microstructures and properties of the coating layer deposited by ultrasonic-assisted laser melt injection have been carried out. However, there are few reports on the effect of ultrasound on the distribution of laser melt injected reinforced particles. In this study, ultrasound is introduced into laser melt injection process to realize the distribution regulation of enhanced particles. Meanwhile, the variability coefficient of Voronoi cell area is adopted to analyze the distribution uniformity of WC particles, which provides a novel approach to evaluate the particle distribution in the laser melt injection layer.

Methods The experimental setup for ultrasonic-assisted laser melt injection (Fig. 1) is mainly composed of fiber-coupled semiconductor laser, cooling system, motion control system, powder feeder, and ultrasonic generator. The substrate used in the experiments is 316L stainless steel plate with size of $\Phi 100 \text{ mm} \times 4.8 \text{ mm}$. The particles used in the laser melt injection are spherical WC particles with phase compositions of WC and W₂C with an average particle size of 75 μm (Fig. 2). Based on the developed experimental setup (Fig. 1), the laser melt injection experiments with and without ultrasound considering various powder feeding rates are carried out. The process parameters are reported in Table 1. After conducting the laser melt injection experiments, the cross-section (perpendicular to the laser scanning direction) and longitudinal section (parallel to the laser scanning direction) of the laser melt injection layer are sampled, polished, and etched. The number density and distribution of WC particles in the melt injection layer are observed and analyzed using optical microscope.

Results and Discussion Aggregation position of WC particles in the coating layer is analyzed using the quadrat method (Figs. 4 and 5). With an increasing powder feeding rate, WC particles gather at the edge of the coating layer without ultrasound, while the number densities of WC particles in different cells of laser melt injection layer are relatively uniform with ultrasound. Meanwhile, a Voronoi diagram of the laser melt injection cross-section is constructed (Figs. 7 and 8). It is found that the area distribution of Voronoi cell is more concentrated with ultrasound (Fig. 9) and variability coefficient of Voronoi cell area is significantly reduced (Fig. 10). These results indicate that ultrasound significantly improves the local aggregation of particles and uniformity of particle distribution. The effects of ultrasonic vibration on the distribution of laser melt injected reinforced particles are revealed. The acoustic cavitation and acoustic flow produced by ultrasound significantly promote the flow of the molten pool and increase the drag force of particles.

WC particles continuously move from the edge of the molten pool to the center of the molten pool with a large drag force. Furthermore, the uniform distribution of particles prevents the stress concentration and inhibits the crack initiation in the laser melt injection layer. Under the condition of non-ultrasound, the macroscopic cracks appear in the laser melt injection layer with a powder feeding rate of 6 g/min, while the macroscopic cracks appear in the laser melt injection layer when the powder feeding rate reaches 8 g/min with ultrasound; accordingly, the number of cracks is significantly reduced (Figs. 11 and 12).

Conclusions In this study, laser melt injected WC particle strengthening layer in a 316L substrate is prepared. The results demonstrate that WC particles gather at the edge of both sides of the laser melt injection layer. Accordingly, numerous macroscopic cracks appear on the surface of the laser melt injection layer without ultrasound with a powder feeding rate of 8 g/min. The application of ultrasonic vibration suppresses the local aggregation of particles and promotes the uniform distribution of WC particles. The Voronoi cell area dispersion coefficient of molten pool decreases by 18.7%–43.52% with ultrasound with powder feeding rates of 2–8 g/min. Meanwhile, improving the WC particle distribution uniformity prevents the initiation of cracks in the coating layer; accordingly, the number of cracks in the laser melt injection layer are significantly reduced with ultrasound.

Key words laser technique; laser melt injection; ultrasound; particle distribution; Voronoi diagram; crack